Experimental demonstration of a compact stellarator magnetic trap using four circular coils

T. Sunn Pedersen,[a] J. P. Kremer, R. G. Lefrancois, Q. Marksteiner, and X. Sarasola[b]
Department of Applied Physics and Applied Mathematics, Columbia University, New York, New York 10027

N. Ahmad
University of California–Berkeley, Berkeley, California 94720

(Received 19 September 2005; accepted 15 November 2005; published online 10 January 2006)

An experimental demonstration of a compact stellarator magnetic trap created from four circular coils is presented. The coil manufacturing and assembly tolerances were on the order of 0.5–1%, far less stringent than most other stellarators. The simplicity, loose mechanical tolerances, and low cost of the trap design makes it feasible for stellarators to be used for a variety of novel physics experiments, in addition to their present use for magnetic confinement fusion. The experiment, the Columbia Non-neutral Torus, has several other desirable features such as no significant internal island chains and the lowest aspect ratio, $A \leqslant 1.9$, of any stellarator built to date. © *2006 American Institute of Physics*. [DOI: 10.1063/1.2149313]

I. INTRODUCTION

A stellarator is a toroidal magnetic confinement device that is characterized by having magnetic surfaces created entirely from external magnets.[1] Traditionally used for fusion research, stellarators possess unique properties that make them attractive as charged particle traps. These advantages include:

- The ability to confine positive and negative particles simultaneously in the same volume, at any degree of neutralization (unlike, e.g., Penning traps);
- The ability to confine particles at arbitrarily low density (unlike tokamaks and other magnetic confinement devices that rely on plasma current to create the required magnetic topology);
- Steady state operation;
- Excellent confinement, at least in the presence of large space charge; and
- Confinement of light charged particles at kinetic energies much higher than those that use electric fields for confinement, such as Penning and Paul traps.

Because of these unique properties, stellarators may be used for a variety of novel physics experiments. The Columbia Non-neutral Torus (CNT) was constructed to explore some of these possibilities, namely the confinement and study of pure electron plasmas, plasmas of arbitrary neutrality, and electron-positron plasmas.[2,3] Other potential uses include the production of neutral antihydrogen (by simultaneous confinement of positrons and antiprotons[2]), allowing a test of charge-parity-time reversal invariance, and basic studies of magnetic reconnection (by introduction of resonant magnetic fields in a stellarator containing plasma[4]).

Stellarators have traditionally been large aspect ratio ($A=5-20$) devices with complicated coils that must be constructed and installed with very high mechanical precision. This makes the use of stellarators for basic physics significantly less attractive. However, several very compact stellarator configurations have been proposed, among them CNT, that have simple coils.[5–9] Compactness, that is, a large confined plasma volume for a given experimental volume (which includes coils and vacuum chamber), is for a toroidal device such as a stellarator synonymous with very low aspect ratio.

In this paper, we report on the first results from CNT: The experimental confirmation of ultralow aspect ratio magnetic surfaces, $A \leqslant 1.9$, created from four circular coils, with no significant internal island chains despite modest construction tolerances. This is by far the lowest aspect ratio stellarator ever built. The lowest aspect ratios achieved in other stellarators were $A \approx 5$.[10,11] It also represents the simplest coil set of any stellarator, in fact simpler than any tokamak. Numerical simulations have shown that the magnetic configuration chosen here is relatively resilient against magnetic field errors such as those caused by coil inaccuracies and other experimentally relevant magnetic perturbations.[5,12] This allowed relatively loose mechanical tolerances to be applied, which greatly facilitated a swift and inexpensive construction. The experimental verification of good magnetic surfaces in CNT therefore demonstrates that stellarators can be easily and inexpensively constructed, yet have a large confining volume of good magnetic surfaces. The paper is organized as follows. First, the CNT experimental configuration is described. The manufacturing tolerances and their practical implications for the construction of CNT are then discussed. The parameters used for the present experiments are given, and the technique used to map out the magnetic surface is briefly described. The primary field line mapping results are presented and compared to numerical calculations, showing that $A \leqslant 1.9$ without significant internal islands was achieved at $B=0.1$ T. Field line mapping results for this con-

[a]Electronic mail: tsp22@columbia.edu
[b]Current address: CIEMAT, Madrid, Spain.

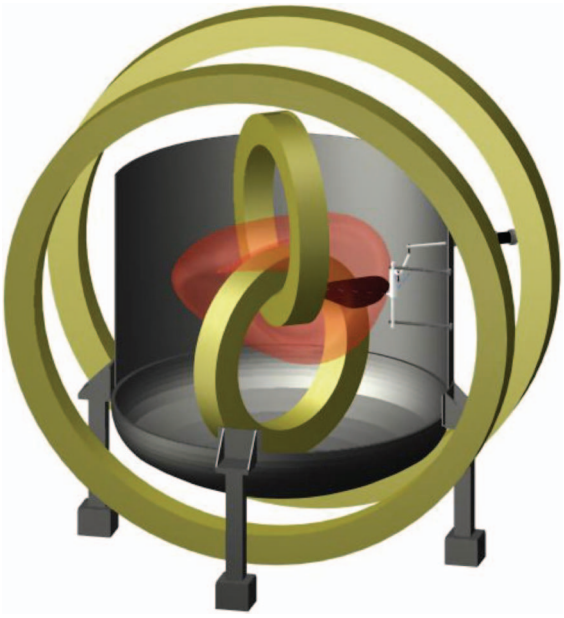

FIG. 1. (Color) A cutaway computer-aided design drawing showing the four coils and the last closed magnetic surface (semitransparent red). The cross-sectional plane mapped here is shown in black.

figuration at lower magnetic field strengths are then presented and discussed. Also presented are results from a somewhat different configuration, which has significant internal island chains.

II. THE CNT EXPERIMENT

CNT has only two pairs of coils, the poloidal field (PF) coils placed outside the vacuum chamber, and the interlocking (IL) coils, placed inside the vacuum chamber. All four coils are simple circular, planar coils, the IL coils with a diameter of 0.81 m, and the PF coils with a diameter of 2.16 m. These four coils together form the magnetic surface configuration, as shown in Fig. 1. CNT can operate in several different coil configurations, by changing the angle between the two IL coils. Three different angles can currently be accommodated in the experiment, 64°, 78°, and 88°. Each of these angles creates a magnetic configuration that is substantially different from the others, in terms of shape, rotational transform, and magnetic shear, as described in Ref. 5. Smaller changes can be effected by varying the ratio α between the currents in the IL and the PF coils, $\alpha = I_{\mathrm{IL}}/I_{\mathrm{PF}}$. The experiments reported on here were performed at a 64° tilt angle and for two values of α, 3.64 and 4.375. The $\alpha = 3.64$ configuration is predicted to have a last closed flux surface (LCFS) aspect ratio of $A = 1.8$, bounded by an external 2/9 island, and to be free of any noticeable island chains inside the LCFS. Throughout this paper, the aspect ratio $A = R/\langle a \rangle$ is calculated numerically using the definition implemented in the VMEC code,[13] which equates $\pi\langle a \rangle^2$ with the toroidally averaged cross-sectional area of the largest flux surface and then defines $2\pi R = V/\pi\langle a \rangle^2$, where V is the volume of the LCFS. The $\alpha = 4.375$ configuration has sizable 2/9 and 2/8 island chains inside the LCFS, and is more sensitive to field errors. However, the LCFS is predicted to have an even lower aspect ratio, $A = 1.50$. This configuration is experimentally convenient because it can be achieved by connecting all four coils in series to a single power supply. It also allows one to study the effects of significant island chains.

III. PRACTICAL IMPLICATIONS OF LOOSE TOLERANCES ON CNT CONSTRUCTION

Most present day stellarators have construction and assembly tolerances on the order from 1×10^{-4} to 1×10^{-3}.[14] To achieve such tolerances, high precision equipment must be used, the manufacturing process must be very carefully monitored, and the assembly becomes a challenging engineering task. Although this can be done successfully, it tends to be a major driver of cost and construction time. In addition to having simple coils it was therefore important for CNT to be resilient to magnetic field errors. This was addressed directly in the optimization of the design of CNT.[5,12] The present configuration of CNT was chosen to have a large volume of good magnetic surfaces and at the same time be resilient against experimentally relevant magnetic field errors. This was achieved through a numerical optimization that included calculations of the sensitivity of the magnetic surface quality and volume to field errors arising from deviations in coil location and orientation, and (to a lesser degree) coil shape. Error fields arising from coil leads and magnetic materials in the vicinity of the device were also considered. These numerical simulations allowed us to determine the acceptable coil manufacturing and assembly tolerances, 2 mm for the IL coils, and 1 cm for the PF coils. Given the size of the coils, (0.405 m radius for the IL coils, 1.08 m radius for the PF coils), the relative tolerances required were 0.5% and 1%, respectively. The loose mechanical tolerances significantly reduced the construction time and cost. Some specific examples are:

- The PF coils were mounted in an inexpensive, easily constructed wood frame.
- A 2 mm discrepancy in the vacuum chamber bolting structure for the IL coils was accommodated by increasing the size of the mating bolt holes on the IL coils by 2 mm rather than attempting to correct the discrepancy.
- After installation, a 2 mm discrepancy in the relative location of the two IL coils was found, seemingly unrelated to the aforementioned bolt hole clearance; because of the loose tolerances, it was not necessary to correct this.
- The assembly of the experiment was performed in a few months primarily by students, and without the use of any specialized high precision tools.
- A larger than specified magnetic permeability $\mu_r > 1.1$ was discovered on some components installed on the vacuum chamber, including a 16.5 in. diameter stainless steel blank flange which was paramagnetic enough to hold a permanent magnet against gravity. Based on the numerical simulations showing error field resilience, it was decided to proceed without attempting to eliminate these error fields.

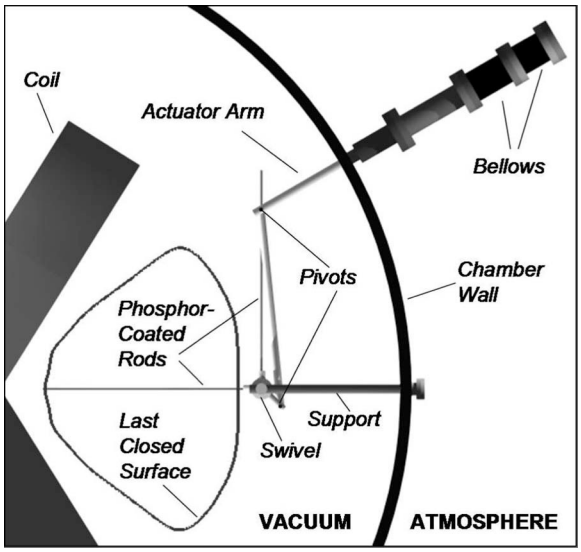

FIG. 2. A computer-aided design drawing showing the details of the rotating rod assembly viewed from the top of the CNT device

IV. MAGNETIC SURFACE MAPPING TECHNIQUE

The magnetic surfaces were mapped out experimentally in CNT using the fluorescent rod method.[15] The setup is shown in Fig. 2. An electron gun, tangent to a given magnetic surface, emits an electron beam nearly parallel to the magnetic field line defining the chosen surface. The electron beam travels along the magnetic field line, deviating slightly due to drifts, forming a drift surface. At $B=0.1$ T, and an electron kinetic energy of 100 eV, the parallel electron gyroradius, $m_e v_\parallel / eB$ is approximately 0.3 mm, so the electrons follow the magnetic field lines very closely, although the drift effects are measurable, as discussed later. Two aluminum rods coated with ZnO:Zn, located far from the electron gun, are swept through the magnetic volume defining a plane of cross section. This cross section, which is shown in Fig. 2 in black, was chosen to be at the $\phi=90°$ symmetry plane of the device. When the aluminum rods intersect the drift surface, the electron beam excites the ZnO:Zn causing a visible bluish-white emission. This emission is then recorded via a 5 s exposure onto a digital camera through a quartz window. In this way, an entire Poincaré map (two-dimensional cross section of a three-dimensional magnetic surface) can be visualized and recorded. Because electron emission only occurs from a filament sufficiently hot to visibly glow, there is inevitably light emitted that illuminates the highly reflective vacuum chamber. In order to eliminate the background light, a second exposure with the electron gun filament glowing, but without electron emission, is taken and subtracted from the first picture. This eliminates almost all background light, except for reflections from sharp shiny objects, which are difficult to completely eliminate. Further enhancement of the images is done by using various filters and contrast enhancement techniques. The background-free magnetic surface pictures for different magnetic surfaces are then added to provide one composite image of the nested magnetic surfaces. For each exposure, landmarks in the picture are used to correct for slight orientation changes of the camera from shot to shot. This ensures proper background subtraction and proper alignment of the surfaces. Landmarks in the pictures also serve to relate the measurements to the numerically calculated Poincaré plots, and to determine the scale of the pictures. Finally, to enhance the clarity of the pictures for reproduction on paper, the pictures are converted into black on white, such that the actual bluish-white emission on a dark background is converted into black on a white background.

V. RESULTS

Field line mapping was performed at the 64° angle between the IL coils for a variety of magnetic field strengths and at several different values of α. Here, we present results from the $\alpha=3.64$ configuration (our baseline configuration) at several different magnetic field strengths, and results from $\alpha=4.375$ at $B=0.07$ T. For these experiments, the vacuum pressure was in the 10^{-8} Torr range, consisting primarily of water vapor, as the chamber was unbaked. This neutral pressure allows electrons to make on the order of 10^3 toroidal transits before hitting a neutral molecule, and hence, neutral effects are negligible. The primary loss mechanism for the electron beam is believed to be collision with the back of the grounded outer casing and mounting structure of the electron gun itself. This "shadowing" effect is clearly seen on most images and is particularly important on the inner magnetic surfaces. A composite image of nested magnetic surfaces for the $\alpha=3.64$ case is seen at the top of Fig. 3. In the middle of Fig. 3, the numerically calculated Poincaré map for the same configuration is shown for comparison. The top image was obtained for an electron beam energy of 100 eV, and at an IL coil current of $I_{\mathrm{IL}}=54$ kA turns, which corresponds to a maximum magnetic field strength of approximately 0.10 T on the magnetic axis. Nested magnetic surfaces are clearly present. There are no detectable island structures or stochastic regions, except at the very edge, where a large $\iota=2/9$ island is present, in agreement with the numerical predictions. When the electron gun was placed outside this island chain, only two or three bright spots would be recorded on the Poincaré images, indicating that the magnetic field lines had become stochastic; this is also in agreement with the numerical calculations. At the bottom of Fig. 3, the experimentally obtained drift surfaces are overlayed on top of the calculated magnetic surfaces. Good agreement is observed, although there are some discrepancies at the plasma edge. A 5 mm inward radial shift (upward on the pictures as shown) has been applied to make the numerically calculated magnetic axis line up with the experimentally determined axis of the drift surfaces. A shift of approximately 5 mm was also needed at $I_{\mathrm{IL}}=37.7$ kA turns to line up the experimentally mapped surfaces. At this slightly lower field (approximately 0.07 T at the maximum field point on the magnetic axis), the degree to which the shift was caused by the curvature drift of the electron beam, rather than an actual shift of the magnetic surfaces, was investigated. This was done by reversing the direction of the currents in all the coils, hence reversing the magnetic field, the curvature drift direction, and the direction of the radial shift of the drift surfaces. For the case of reversed field, no shift was needed to align the experimental

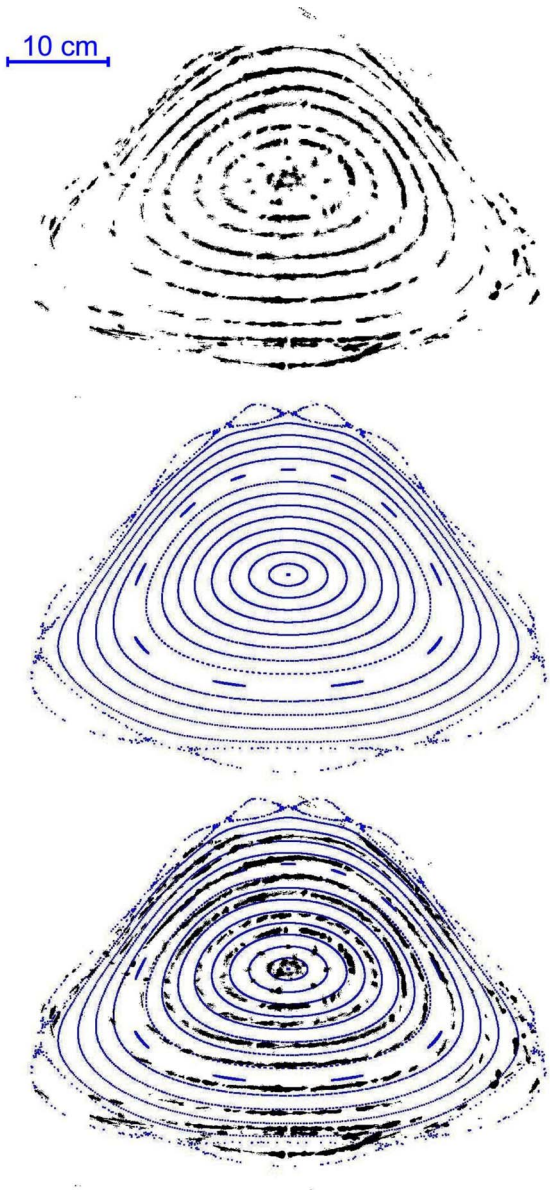

FIG. 3. (Color online) Field line mapping results for the $\alpha=3.64$ configuration at $B=0.10$ T. Top: A composite image showing the nested drift surfaces, and the bounding 2/9 island structure. Middle: The numerically calculated magnetic surfaces on the same scale. Bottom: The composite image overlayed on the numerical surfaces. The composite image was shifted 5 mm inward radially (up on these pictures) to line up the two axes. The scale is indicated in the top left-hand corner

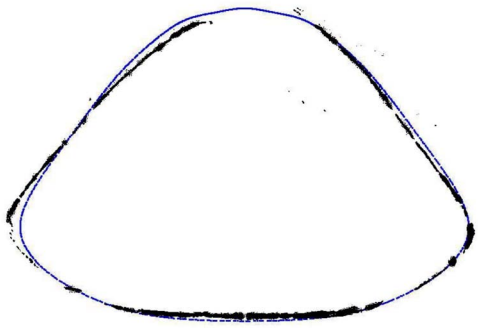

FIG. 4. (Color online) The largest closed magnetic surface found experimentally, superimposed on a numerically calculated surface.

and numerical axes. Since the two sets of drift surfaces (forward and reversed fields) should be displaced symmetrically around the magnetic surfaces (one set of drift surfaces radially out, one set radially in), it is concluded that there is an approximately 2.5 mm drift surface shift, and an actual discrepancy between the experimentally created magnetic surfaces and those calculated numerically, of approximately 2.5 mm, with the measured surfaces displaced inward (towards the axis of the vacuum chamber). In the forward field configuration, the two shifts add up, whereas they cancel in the reversed field configuration. The approximate 2.5 mm axis discrepancy is well within the cumulative uncertainties due to the combination of uncertainty in the geometry of the IL coils (which were specified with a 2 mm tolerance), the vacuum chamber (with similar tolerance) and in α. The uncertainty in α is estimated to be 1%, due to calibration uncertainties in the coil currents. Figure 4 shows the largest good magnetic surface found experimentally, with the closest matching calculated surface superimposed. There are shape differences on the order of 1 cm between the two (also visible in Fig. 3), including a somewhat broken symmetry of the magnetic surface shape. These are presumably due to field errors caused by the large tolerances. However, the field errors do not cause a loss of confined volume or any measurable island chains in the interior—the volumes are nearly identical. Using the numerical code, the aspect ratio of this magnetic surface is calculated to be $A=1.89$. The numerical calculations predict that a slightly larger closed magnetic surface exists, yielding an aspect ratio of 1.8, but it was not possible experimentally to place the electron gun accurately enough to map out this surface. It may be that this numerically calculated surface has become part of the 2/9 island chain. Thus, we conclude that the aspect ratio of the magnetic configuration is $A \leqslant 1.9$. This is by far the lowest aspect ratio of any stellarator actually constructed. The images shown in Figs. 3 and 4 are among the sharpest and highest quality obtained. For maximum sharpness, the e-beam current and e-beam acceleration voltage had to be carefully adjusted. If the beam current (adjusted by changing the filament temperature) was too small, images would be too faint. If too large, images would be very bright, but somewhat blurry. Large beam acceleration voltage (100 V or greater) would lead to bright, sharp images, whereas lower beam voltage would lead to less focused spots. These observations can be explained by beam defocusing due to the self-repulsion of the beam electrons, which is more severe for low beam energy and high beam current. On the other hand, larger beam voltage implies larger drift deviations so the optimum was found to be 100 V. Finally, the focus of the beam was observed to strongly improve when the e-gun alignment with the magnetic field was improved.

Field line mapping for $\alpha=3.64$ was also performed at a range of lower magnetic field strength values to determine the effects on the magnetic topology. In order to investigate the effects of magnetic field strength on plasma confinement

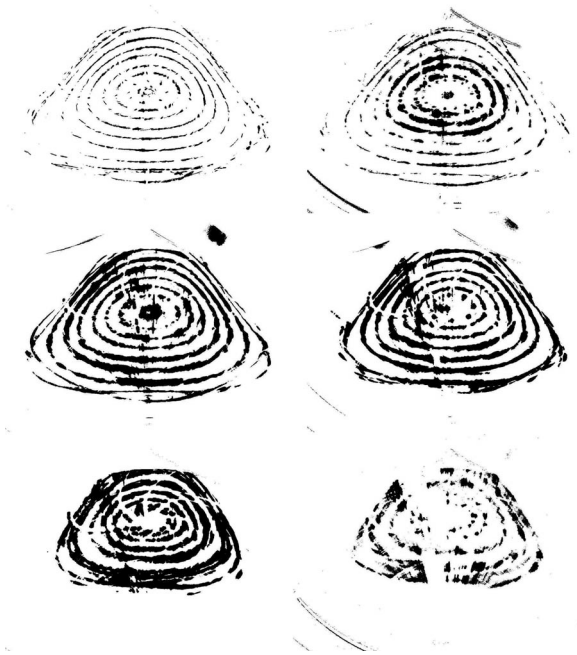

FIG. 5. Results of B-field scan for $\alpha=3.64$. Top left: $B=0.10$ T; top right: $B=0.06$ T; middle left: $B=0.030$ T; middle right: $B=0.015$ T; bottom left: $B=0.0074$ T; and bottom right: $B=0.0041$ T.

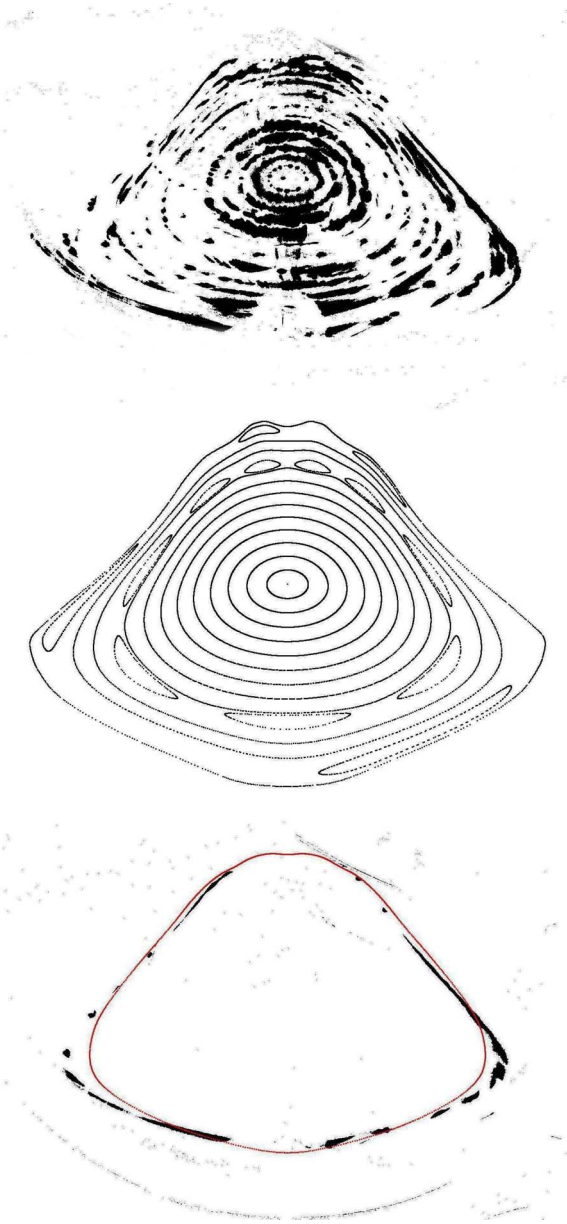

FIG. 6. (Color online) Field line mapping results for the $\alpha=4.375$ configuration at $B=0.07$ T. Top: A composite picture of the experimentally obtained nested magnetic surfaces; middle: the numerically calculated surfaces; and bottom: the LCFS obtained experimentally with the closest fitting numerical surface overlayed.

and stability, one should verify that the magnetic topology remains unchanged as the magnetic field strength is varied. For sufficiently large magnetic field strengths, one would expect this to be the case, as long as the field is low enough not to induce coil distortions due to electromagnetic forces. Topological changes are expected to occur at very low magnetic field strengths because Earth's magnetic field, and other permanent magnetic fields arising from magnetized material in the vicinity of the experiment, eventually become significant as the fields produced by the coils are lowered. In Fig. 5, we show composite magnetic surface images for $B=0.10$, 0.06, 0.030, 0.015, 0.0074, and 0.0041 T. For all of these, $\alpha=3.64$, and the electron beam energy was 100 eV, except for $B=0.0041$ T, as discussed in the following. The lower field images are generally brighter (more highly exposed), but not as sharp as those presented for $B=0.1$ T, primarily due to the beam-defocusing effect, although at the lowest fields, there may be finite Larmor radius effects as well. For the $B=0.06$ T case, the effects of realignment and retuning of the electron beam are clearly visible, with inner surfaces brighter and less focused than outer surfaces. At $B=0.030$ T, nested magnetic surfaces of the same shape, topology and size as those in Fig. 3 are seen. At $B=0.015$ T, minor changes in the location and symmetry of the outer magnetic island chain begin to appear but the confined region is only slightly reduced. At $B=0.0074$ T, the confined region has decreased appreciably, although a significant volume of good magnetic surfaces is still present. A new island chain also appears. At this value of B, the parallel electron Larmor radius is 3.2 mm. Drift surface deviations from magnetic surfaces are on the order of 25 mm, and Earth's magnetic field (0.0005 T) is a 0.7% perturbation. Thus, the significant shape deviations and apparent loss of outer magnetic surfaces are to be expected due to a combination of finite Larmor radius, ∇B drift, and static magnetic field error effects. At $B=0.0041$ T, the image quality is poor. In this case, the beam energy had to be lowered to 18 eV in order to map out the magnetic surfaces. At 100 eV beam energy, only a small inner core of surfaces could be mapped out. The lowered beam energy produced large beam defocusing and less fluorescence than at 100 eV. Despite the poor image quality, it appears that magnetic surfaces are still seen, with similar topology and size as for $B=0.0074$ T. Based on these results we conclude that the CNT $\alpha=3.64$ topology is essentially unchanged in the range $0.015\ \text{T}<B<0.10$ T. We also conclude that a significant, but reduced volume of good magnetic surfaces exists even for $0.0041\ \text{T}\leqslant B<0.015$ T. In Fig.

6 we show a composite image obtained at $B=0.07$ T for $\alpha=4.375$, together with the numerically calculated surfaces for this configuration, and an overlay of the experimental LCFS overlayed with the closest fitting numerically calculated surface. Although $\alpha=4.375$ is predicted to have several sizable internal island chains and significantly higher error field sensitivity, this configuration is of interest for three reasons. First, it has an even lower predicted aspect ratio, $A=1.50$, than the baseline configuration. Second, because of the presence of the internal island chains, the configuration can be used to study the effects of islands on transport, confinement, and stability. Third, this current ratio can be achieved with all four coils connected in series from a single power supply, which is convenient, and fully eliminates any uncertainty in α. The field line mapping system, which was designed to work optimally for the $\alpha=3.64$ configuration, was unable to fully map the outer magnetic surfaces of the $\alpha=4.375$ configuration due to the larger major radius and larger outer magnetic surfaces. In particular, there is a circular region without emission because the mounting structure for the rods was not coated with ZnO:Zn. There is general agreement with the numerically calculated surfaces, except near the edge where significant deviations of several centimeters are seen. Comparing the experimentally obtained LCFS to the most closely matching numerical surface, we estimate the aspect ratio to be $A\leqslant 1.82$, i.e., slightly lower than for $\alpha=3.64$ but significantly higher than predicted numerically. The most likely explanation for the apparent lack of outer surfaces is that these surfaces have become stochastic due to field errors. As mentioned previously, this configuration did not show the same resilience to field errors as $\alpha=3.64$ did, presumably because the 2/9, 4/17, and 2/8 island chains all are located near the plasma edge.

VI. DISCUSSION

The results presented demonstrate the first experimental creation of an ultralow aspect ratio stellarator, $A\leqslant 1.9$, without significant internal islands. Given the simple coil configuration and loose mechanical tolerances, it shows that stellarators can be compact (i.e., ultralow aspect ratio), inexpensive, and relatively easy to construct and assemble, allowing them to be used for basic physics experiments such as CNT. These same properties are also highly desirable for any economical fusion reactor device. However, a stellarator fusion reactor also requires good confinement of high beta plasma, and good confinement of the energetic charged fusion products, such as the alpha particles produced in deuterium-tritium fusion. These requirements were not considered in the optimization of CNT, as they are not particularly important for the basic research mission of the device.[5] Calculations have shown that CNT has a large helical ripple,[16] which presumably precludes good fusion alpha confinement and it would therefore likely not be a good candidate for a burning fusion plasma reactor. Nonetheless, it may serve as a useful starting point for a numerical search for a compact, simple coil stellarator with good fusion performance and relatively loose mechanical tolerances.

ACKNOWLEDGMENTS

The authors would like to thank Matthias Otte and Victor Sakaguchi for providing detailed information and help regarding the electron gun and phosphorescent rods, and to Stephen Paul for help with the bellows for the electron gun. The authors would also like to thank Allen Boozer and Harry Mynick for useful discussions, and Wayne Reiersen, Fred Dahlgren, and Neil Pomphrey for help with the CNT design. The CNT program is supported by the United States Department of Energy, Grant No. DE-FG02-02ER54690, and the National Science Foundation, Grant No. PHY-0317359.

[1] A. H. Boozer, Phys. Plasmas **5**, 1647 (1998).
[2] T. S. Pedersen and A. H. Boozer, Phys. Rev. Lett. **88**, 205002 (2002).
[3] T. S. Pedersen, A. H. Boozer, W. Dorland, J. P. Kremer, and R. Schmitt, J. Phys. B **36**, 1029 (2003).
[4] A. H. Boozer (private communication, 2005).
[5] T. S. Pedersen, A. H. Boozer, J. P. Kremer, R. Lefrancois, F. Dahlgren, N. Pomphrey, and W. Reiersen, Fusion Sci. Technol. **46**, 200 (2004).
[6] C. Gourdon, D. Marty, E. K. Maschke, and J. P. Dumont, *Plasma Physics and Controlled Nuclear Fusion Research* (International Atomic Energy Agency, Vienna, Austria, 1969), p. 849.
[7] T. N. Todd, Plasma Phys. Controlled Fusion **32**, 459 (1990).
[8] P. E. Moroz, Phys. Rev. Lett. **77**, 651 (1996).
[9] P. E. Moroz, Phys. Lett. A **243**, 60 (1998).
[10] S. Knowlton *et al.*, J. Fusion Energy **12**, 261 (1993).
[11] K. Nishimura *et al.*, Fusion Technol. **17**, 86 (1990).
[12] J. P. Kremer, T. S. Pedersen, N. Pomphrey, W. Reiersen, and F. Dahlgren, AIP Conf. Proc. **692**, 320 (2003).
[13] S. P. Hirshman and D. K. Lee, Comput. Phys. Commun. **39**, 161 (1986).
[14] M. Wanner, J.-H. Feist, H. Renner, *et al.*, Fusion Eng. Des. **56–57**, 155 (2001).
[15] R. Jaenicke, E. Ascasibar, P. Grigull, I. Lakicevic, A. Weller, M. Zippe, H. Hailer, and K. Schworer, Nucl. Fusion **33**, 687 (1993).
[16] N. Pomphrey (private communication, 2002).